International Journal of Climatology 38 (8): 3233-3249 (2018)

Title: Estimation of near-surface air temperature lapse rates over continental Spain and its mountain areas

Running title: Air temperature lapse rates over continental Spain

Authors: Navarro-Serrano, F.[1]; López-Moreno, J.I.[1]; Azorin-Molina, C.[2]; Alonso-González, E.[1]; Tomás-Burguera, M.[3]; Sanmiguel-Vallelado, A.[1]; Revuelto, J.[4]; Vicente-Serrano, S.M.[1]

[1]Department of Geoenvironmental Processes and Global Change, Pyrenean Institute of Ecology, CSIC, Zaragoza, Spain.

[2]Regional Climate Group, Department of Earth Sciences, University of Gothenburg, Gothenburg, Sweden.

[3]Estación Experimental Aula Dei, CSIC, Zaragoza, Spain.

[4]Météo-France, CNRS, CNRM, UMR3589, CEN, Grenoble, France.

Correspondence to: Navarro-Serrano, F. Department of Geoenvironmental Processes and Global Change, Pyrenean Institute of Ecology, CSIC (Spanish Research Council), Campus de Aula Dei, P.O. Box 202, Zaragoza 50080, Spain. E-mail: fnavarro@ipe.csic.es. Phone number: (+34) 976 369 393. Fax: 974 363 222.

Abstract:

Although the mean environmental lapse rate (MELR) value (a linear decrease of –6.5°C km^{-1}) is the most widely used, near-surface (i.e., non-free-atmosphere) air temperature lapse rates (NSLRs; measured at ~1.5 m height) are variable in space and time because of their dependence on topography and meteorological conditions. In this study we conducted the first analysis of the spatial and temporal variability of NSLRs for continental Spain and their relationship to synoptic atmospheric circulation (Circulation Weather Types – CWTs), focusing on major mountain areas including the Pyrenees, Cantabrian, Central, Baetic, and Iberian ranges.

The results showed that the NSLR varied markedly at spatial and seasonal scales, and depended on the dominant atmospheric conditions. The median NSLR values were weaker (less negative) than the MELR for the mountain areas (Pyrenees –5.17 °C km^{-1};

Cantabrian Range –5.22 °C km^{-1}; Central Range –5.78 °C km^{-1}; Baetic Range –4.83 °C km^{-1}; Iberian Range –5.79 °C km^{-1}) and for the entire continental Spain (–5.28°C km^{-1}). For the entire continental Spain the steepest NSLR values were found in April (–5.80°C km^{-1}), May (–5.58°C km^{-1}) and October (–5.54°C km^{-1}) because of the dominance of northerly and westerly advections of cold air. The weakest NSLR values were found in July (–4.67°C km^{-1}) and August (–4.78°C km^{-1}) because of the inland heating, and in winter because of the occurrence of thermal inversions. As the use of the MELR involves the assumption of large errors, we propose 1 Zonal, 12 Monthly, 11 CWTs, and 132 hybrid Monthly-CWTs NSLRs for each of the mountain ranges and for the entire continental Spain. More regional studies are urgently needed to accurately assess the NSLR as a function of atmospheric circulation conditions.

Key words: *Lapse rate; Air temperature; Mountain climate; Weather types; Complex terrain; Spain*

1. Introduction

Although near-surface (i.e., ~1.5 m elevation above the ground) air temperature is not a challenging climate variable to extrapolate spatially, modeling in mountain areas can be associated with substantial uncertainties because of the complex topography (Barry, 1992; Whiteman et al., 1999; Minder et al., 2010). In mountain areas the most common procedure for modeling near-surface air temperature involves using air temperature lapse rate, which is defined as the ratio of air temperature change per elevation unit, generally measured in degrees (ºC) per kilometer (km^{-1}) (Fang and Yoda, 1988). The most widely used spatio-temporal fixed air temperature lapse rate is the mean

environmental lapse rate (MELR: –6.5°C km^{-1}); this parameter was presented by Barry and Chorley (1987) as a global lapse rate calculated for the free atmosphere air temperature, and not for near-surface air temperature. However, caution is required in use of the MELR because of the spatio-temporal variability of near-surface air temperature lapse rates (Pepin et al., 1999, 2011; Rolland, 2003; Lundquist and Cayan, 2007; Blandford et al., 2008; Minder et al., 2010; Dumas, 2013; Kattel et al., 2013; Miró et al., 2017), especially in areas covered by ice or snow (Braun and Hock, 2004). This is because the fixed MELR assumes no changes among seasons, synoptic conditions, or topographic complexity (Barry, 1992).

Near-surface temperature lapse rates (NSLRs) are linear observed ratios between temperature and elevation, and they can be calculated for a specific or aggregated time and space. They are readily calculated, but this requires fine temporal and spatial data resolution to enable most of the variability to be represented. NSLR have been widely used in scientific fields including Glaciology, Hydrology, Forestry, Agricultural Sciences, and Ecology (Martinec et al., 1983; Running et al., 1987; Barringer, 1989; Pepin, 2001; Rolland, 2003; Hanna et al., 2005; Blandford et al., 2008; Minder et al., 2010; Immerzeel et al., 2014). NSLRs can be calculated from maximum ($NSLR_{max}$), minimum ($NSLR_{min}$) or mean ($NSLR_{mean}$) air temperatures, in line with Harlow et al. (2004) and Minder et al. (2010). Many scientists only used elevation to calculate NSLR (e.g., Immerzeel et al., 2014; Heynen et al., 2016), but air temperature changes are not only due to elevation. Therefore, more complex approaches including regional multiple regression analyses are needed to isolate the effect of elevation on air temperature from other geographical and topographical variables (e.g., latitude, longitude, slope, and continentality), which strongly affect the spatial variability of near-surface air

temperatures (Bolstad et al., 1998). In doing so, it may become possible to determine the specific elevation effect on the distribution of temperatures. Observed NSLRs and fixed MELRs can differ because the distribution of air temperatures are strongly dependent on the topography (Barry, 2001; Pepin, 2001; Marshall et al., 2007) and other atmospheric parameters such as air humidity, wind speed and wind direction, cloud cover, and radiative conditions (Kattel et al., 2013). Moreover, NSLRs vary between day and night because of the heat flux exchanges between the atmosphere and the ground surface (Gardner et al., 2009). In most situations near-surface air temperatures drop with increasing elevation. However, stable atmospheric conditions can reverse this effect forming valley cold pools (i.e., thermal inversions with warm air above, and cold air near the valley floor), especially during the winter months (e.g. Barry, 1992; Whiteman et al., 1999; Pagès and Miró, 2010). Cold-air pools are formed as a result of both cooling of the ground due to long-wave radiation and nocturnal down-slope winds, but more complex mechanisms help/avoid in their formation (Whiteman et al., 1999).

Several studies have reported significant temporal variability in NSLR at daily and seasonal scales in various mountain regions including the Rocky (Kunkel, 1989; Pepin and Losleben, 2002; Blandford et al., 2008) and Appalachian (Bolstad et al., 1998) mountains in the USA, in China (Fang and Yoda, 1988; Tang and Fang, 2006; Du et al., 2010), the Himalayan mountains (Kattel et al., 2013; Immerzeel et al., 2014), the Alps (Rolland, 2003; Dumas, 2013; Kirchner et al., 2013; Nigrelli et al., 2017), and polar areas (Marshall et al., 2007). These studies have reported steeper NSLRs under unstable atmospheric conditions, and marked differences in NSLR have been found as a function of synoptic conditions (Pepin et al., 1999, 2011; Pepin, 2001; Blandford et al., 2008; Holden and Rose, 2011; Kirchner et al., 2013; Miró et al., 2017). These findings

indicate that these effects need to be taken into account when analyzing the temporal and spatial evolution of the NSLR.

Continental Spain (CS) and its mountain areas is a topographically complex region, and several studies have investigated the effect of changes in the frequency of weather types on various climate parameters (Trigo and Dacamara, 2000; Tomás et al., 2004; García-Herrera et al., 2007; López-Moreno and Vicente-Serrano, 2007; Buisan et al., 2015a). However, the spatio-temporal variability of NSLRs in the region has only been investigated in a limited number of local studies in the Pyrenees (Puigdefábregas, 1969; Pepin and Kidd, 2006; Pagès and Miró, 2010). These few previous studies have analyzed the effects of regional topography on NSLRs comparing atmospheric model results with observed data, but none of them have investigated how different circulation weather types affect seasonal patterns of NSLR in the main mountain areas of CS. In addition, previous investigations analyzed daily maximum temperature lapse rates ($NSLR_{dmax}$), daily minimum temperature lapse rates ($NSLR_{dmin}$) and daily mean temperature lapse rates ($NSLR_{dmean}$) separately, following Harlow et al. (2004) and Minder et al. (2010). It is important to clarify the sign of lapse rates. A steeper lapse rate indicates a more negative and rapid decrease in air temperature with elevation, while a weaker rate indicates less negative or even positive changes in air temperature with elevation. To assess the similarity of NSLRs among the months, weather types, and regions considered in the present work, Wilcoxon-Mann-Whitney test (Wilcoxon, 1945) was used.

This study is the first attempt to investigate NSLR across CS with focus on assessing the seasonal and synoptic variability of this parameter over the major mountain ranges. The spatio-temporal analysis of NSLRs is strongly needed in Spain because the

complex terrain makes air temperature challenging to predict. In addition, this approach helps to improve hydrologic models and snow simulations what is particular useful in areas subject to water scarcity and desertification, as is the case of Spain (Vicente-Serrano, 2007; García-Ruiz et al., 2011). The aims of the study are: (i) to define annual and seasonal NSLR reference values; (ii) to quantify the effect of seasonality and different weather types on NSLR at a regional scale; and (iii) to assess the uncertainty associated with the use of different reference NSLR, including the MELR (–6.5°C km^{-1}) and other NSLR defined in this study, based on seasonality and weather types.

2. Data

2.1 Study area

CS is characterized by its complex topography, with many mountain ranges located within the area (Fig. 1). The average elevation of the entire CS is 688 m above sea level (m a.s.l.; standard deviation = 399 m), and the highest elevation point is the Mulhacén Peak (Baetic Range) at 3,479 m a.s.l. The climate of CS is mainly influenced by the Atlantic Ocean, the Mediterranean Sea, and its proximity to both subtropical and temperate air mass. The climatic conditions are mainly humid and temperate in the North Atlantic area (defined as *Cf* in the Köppen classification), and dry and warm in the remainder (*Cs* in the Köppen classification). Different climates occur depending on exposure to the Atlantic Ocean or the Mediterranean Sea, the continentality, and the complex topography of the region. Based on the variability of annual rainfall, Rodríguez-Puebla et al. (1998) identified four main precipitation regions across Spain: northwest, south-southwest, the Mediterranean coast, and the Cantabrian coast. Total annual precipitation ranges from more than 2,000 mm in the northern slopes of the Cantabrian Range, the Pyrenees and the Central Range to less than 400 mm in the driest

areas of the Baetic and the Iberian ranges (AEMET, 2011). In this study we analyzed the NSLR for the entire CS, with focus on its five major mountain ranges (Fig.1): (1) the Pyrenees, in the northeast; (2) the Cantabrian Range, in the northwest; (3) the Central Range, in the middle west; (4) the Baetic Range, in the southeast; and (5) the Iberian Range, in the middle east. The elevation ranges and distributions, and the size of the study area for the five mountain ranges are summarized in Table 1.

2.2. Air temperature data and Digital Elevation Model

Complete records of daily maximum and minimum near-surface (i.e., ~1.5 m height) air temperature were obtained from the Spanish State Meteorological Agency (AEMET) database. A total of 3,950 air temperature series were available for the entire CS (the distribution of weather stations is shown in Fig. 1). Among them, 664 are located in the Pyrenees, 455 in the Cantabrian Range, 376 in the Central Range, 650 in the Baetic Range, and 390 in the Iberian Range. This is the densest network of weather stations available for calculating NSLR across CS. The majority of weather stations are located in the lower parts of valleys (< 1500 m a.s.l.), with < 5% being located high mountain areas (see the distribution in Fig. 1; and elevation ranges in Fig. 2).

Near-surface air temperature data were obtained based on recommendations of the World Meteorological Organization (WMO, 2008) in relation to radiation shields and height above the ground. Two types of high quality thermometer that meet the WMO requirements for a measurement range of –30 to 50°C were used in the station network (Buisan et al., 2015b), and were protected from solar radiation by Stevenson radiation shields. Geographic variables (i.e., latitude, longitude and elevation) were derived from metadata supplied by the AEMET, and validated using geographical information systems (GISs). With the aim of maximizing long-term analysis and a good station

density, we analyzed the period from December 1979 to August 2015. The start and end dates for data acquisition from each station, and the number of data gaps varied over time, with the largest number of daily observations available since the 1990s (Fig. 2). A digital elevation model (DEM) having a pixel size of 900 square meters, derived from the Shuttle Radar Topography Mission (SRTM) (Farr et al., 2007), was used to calculate the distance of each weather station to the coast. The hydrographic network was obtained from the IECA website [https://www.juntadeandalucia.es/institutodeestadisticaycartografia/DERA/index.htm; last accessed 2 November 2017], which is derived from the World Map Vector (VMap0) developed by United States Defense Mapping Agency (USDMA, 2000).

3. Methods

3.1 Quality Control and Preprocessing

Daily maximum and minimum near-surface air temperature data were subject to quality control to ensure data accuracy. Large weather station networks can contain data outliers introduced by errors during the conversion of manual records. Therefore, we applied the robust quality control procedure described by Tomás-Burguera et al. (2016), involving the removal of questionable records according to Durre et al. (2010). Following the quality control process a total of 21.21×10^6 daily maximum and 21.19×10^6 daily minimum records were available covering the entire CS and its mountain areas for the December 1979 to August 2015 period.

3.2 Circulation weather type classification

Daily weather types over CS were determined using the Jenkinson and Collison (1977) classification, which is based on the Lamb's weather type scheme (Lamb, 1972). This

196 method is based on daily sea level pressure (SLP) data from 16 grid points covering the
197 entire Iberian Peninsula (Fig. 3). The SLP data were obtained from the NCEP-NCAR
198 reanalysis (5º x 5º longitude – latitude) dataset (Basnett and Parker, 1997)
199 [https://climatedataguide.ucar.edu/climate-data/ncar-sea-level-pressure, last accessed 2
200 November 2017]. Equations and rules applied for 40ºN are:

201 $SF \text{ (Southerly Flow)} = 1.305[0.25(p5 + 2 \times p9 + p13) – 0.25(p4 + 2 \times p8 + p12)]$

202 $WF \text{ (Westerly Flow)} = [0.5(p12 + p13) – 0.5\ (p4 + p5)]$

203 $ZS \text{ (Meridional Vorticity)} = 0.85 \times [0.25(p6 + 2 \times p10 + p14) – 0.25(p5 + 2 \times p9 + p13)$
204 $– 0.25(p4 + 2 \times p8 + p12) + 0.25(p3 + 2 \times p7 + p11)]$

205 $ZW \text{ (Zonal Vorticity)} = 1.12 \times [0.5(p15 + p16) – 0.5(p8 + p9)] – 0.91 \times [0.5(p8 + p9) –$
206 $0.5(p1 + p2)]$

207 $F \text{ (Total Flow)} = 0.5 \times (SF^2 + WF^2)$

208 $Z \text{ (Total Vorticity)} = ZS + ZW$

209 , where:

210 *p* is the sea level atmospheric pressure value (in hPa) at grid-point number position.

211 Rules:

212 (i) If |Z| is less than F, flow is essentially straight, corresponding to a Lamb directional
213 type, e.g. W

214 (ii) If |Z| is greater than 2F, then the pattern is strongly cyclonic or anticyclonic,
215 corresponding to Lamb's C (Cyclonic) and A (Anticyclonic) types.

(iii) If |Z| lies between F and 2F, then the flow in moderately cyclonic or anticyclonic, corresponding to a Lamb hybrid type, with the direction specified, e.g. CNW (Cyclonic – Northwest)

(iv) If F is less than 6, there is light indeterminate flow, corresponding to Lamb's U type (Unclassified)

The Jenkinson and Collison's weather type classification has been widely used and successfully applied to the Iberian Peninsula (e.g., Goodess and Palutikof, 1998; Spellman, 2000; Trigo and Dacamara, 2000; López-Moreno and Vicente-Serrano, 2007; to name but a few). The classification includes 27 circulation weather types (CWTs) including: unclassified (U); anticyclonic (A); cyclonic (C); 8 directional CWTs (N, NE, E, SE, S, SW, W and NW); and 16 hybrid cyclonic or anticyclonic and directional CWTs (CN, CNE, CE, CSE, CS, CSW, CW, CNW, AN, ANE, AE, ASE, AS, ASW, AW and ANW). To assess the relationships between CWTs and NSLR, the 16 hybrid CWTs were classified according to their directional flow following Trigo and DaCamara (2000), i.e. simplifying the interpretation of the results to 2 pure (A and C) and 8 directional (N, NE, E, SE, S, SW, W and NW) CWTs. We also defined a severe anticyclonic type (A+) as a third pure CWT in order to identify days having strong stability . A day was classified as Severe Anticyclonic (A+) if: (i) the day was classified as pure Anticyclonic (A), and (ii) SLP in *p8* was > 1,030 mb.

In addition, unclassified (U) days were reclassified by three rules based on SLP values of *p8* gridpoint, following the procedure adopted by Rasilla et al. (2002): (i) if *p8* < 1,020 mb, the day was reclassified as pure Cyclonic (C); (ii) if *p8* is between 1,020 and 1,030 mb, the day was reclassified as pure Anticyclonic (A); (iii) if *p8* > 1,030 mb, the day was reclassified as Severe Anticyclonic (A+).

3.3 Daily near-surface air temperature lapse rate (NSLR)

The daily maximum near-surface air temperature lapse rate ($NSLR_{dmax}$) and the daily minimum near-surface air temperature lapse rate ($NSLR_{dmin}$) were calculated for each mountain range and for the entire CS. $NSLR_{dmax}$ and $NSLR_{dmin}$ were computed using all available simultaneous data (Fig. 2). The daily average number of weather stations used in the regression was: 279 in the Pyrenees; 179 in the Cantabrian Range; 150 in the Central Range; 275 in the Baetic Range; 167 in the Iberian Range; and 1,623 for the entire CS. The daily average equated to one weather station every 266 km^2 in the Pyrenees, 362 km^2 in the Cantabrian Range, 426 km^2 in the Central Range, 337 km^2 in the Baetic Range, 373 km^2 in the Iberian Range, and 301 km^2 throughout the entire CS. Figure 2 shows that lower elevation ranges (i.e., 0–500 m a.s.l. and 500–1000 m a.s.l.) were well represented, which contrast with the low density of weather stations at higher elevations for all mountain ranges.

Following the procedure proposed by Rolland (2003), multiple regressions were used to compute daily maximum and minimum NSLRs from maximum and minimum air temperatures (Tmax and Tmin, respectively) of stations. Thus, it can be quantified the effect of elevation on air temperature without including other topographic and geographic variables (Bolstad et al., 1998; Blandford et al., 2008; Gardner et al., 2009). For calculating $NSLR_{dmax}$ and $NSLR_{dmin}$, the elevation of each station along with other geographic variables including latitude, longitude, and distance to the sea were taken into account. The distance of each station to the nearest river (until order 4 according to Gravelius classic system, being order 1 the largest stream) was also recorded as a proxy in order to account for the influence of relative micro-topographic features, such as

thermal inversions and cold air pools (Lookingbill and Urban, 2003; Whiteman et al., 2004). Equation 1 summarizes this methodology:

$$Tmax' \text{ and } Tmin' = a_0 + a_1Elev + a_2Lat + a_3Lon + a_4Sea + a_5Riv + e \quad \text{(Eq. 1)}$$

where *Tmax'* and *Tmin'* are the maximum and minimum near-surface air temperatures, respectively (in °C); *Elev*, *Lat*, *Lon*, *Sea*, and *Riv* are the elevation above sea level (in m a.s.l.), latitude (in UTM), longitude (in UTM), distance to the sea (in km), and distance to the nearest river (in km), respectively; *e* is a regression error; and a_1, a_2, a_3, a_4, and a_5 are the regression coefficients, with a_1 corresponding to the daily maximum ($NSLR_{dmax}$) or minimum ($NSLR_{dmin}$) lapse rate, following the procedure of Rolland (2003). Confidence intervals (95%) for each $NSLR_{dmax}$ and $NSLR_{dmin}$ were calculated. The mean daily average near-surface air temperature lapse rate ($NSLR_{dmean}$) was obtained by averaging $NSLR_{dmax}$ and $NSLR_{dmin}$. The $NSLR_{dmean}$ was computed on a daily basis and then grouped by months and CWTs, with the aim of developing reference NSLR values (i.e., 1 Zonal, 12 Monthly, 11 CWTs, and 132 Monthly–CWTs) from median values. The Wilcoxon-Mann-Whitney is a non-parametric statistic test that allows the comparison between two independent series to know the similarity between their distributions. In this work, we compare the total amount of daily NSLR, distributed by: (1) months in the same study area (396 combinations); (2) study areas in the same month (180 combinations); (3) CWTs in the same study area (396 combinations); and (4) study areas in the same CWTs (180 combinations).

3.4. Near-surface lapse rate validation

To quantify the accuracy of the proposed NSLR reference values, a validation process was applied. This was based on the use of potential temperature; i.e., the air temperature

at a common sea level reference applying lapse rates (Marsh, 2009). The following steps were applied: (i) the daily random selection of 20% of weather stations available for a subset of the study period (1981–2010). This subset period was chosen to adapt the analysis to a normalized climate period of 30 years; (ii) the sea level potential daily maximum and minimum air temperature was estimated for each of the randomly selected weather stations using a daily multiple regression model (Eq. 1), based on the other 80% of stations; (iii) sea level potential mean air temperature was calculated averaging sea level potential daily maximum and minimum air temperature data calculated (see step ii); and (iv) real elevation estimated air temperature was calculated to each station from the sea level potential mean air temperature by applying different NSLR proposed reference values (Zonal, Monthly, CWTs, and hybrid Monthly–CWTs NSLRs; explained in section 3.3), and the widely used MELR.

Mean absolute error (MAE) statistics were calculated from the difference between real observed air temperature and estimated (see step iv above), and was summarized for winter (December–February: DJF), spring (March–May: MAM), summer (June–August: JJA), and autumn (September–November: SON).

4. Results

4.1 Climatology of the $NSLR_{dmean}$

Figure 4 shows the daily mean air temperature lapse rate ($NSLR_{dmean}$) across the CS and its mountain areas for December 1979–August 2015. We found a marked variability in daily values (measured as the standard deviation), and large differences between each of the five mountain areas and the CS. This variability ranged from 2.06°C km^{-1} for the Central Range to 1.40°C km^{-1} for the Pyrenees, being 1.15°C km^{-1} for the entire CS.

For the majority of days the daily $NSLR_{dmean}$ was weaker than the MELR, especially in the Pyrenees and the Iberian Range. The median daily zonal values (Table 2) were –5.17°C km^{-1} for the Pyrenees, –5.22°C km^{-1} for the Cantabrian Range, –5.78°C km^{-1} for the Central Range, –4.83°C km^{-1} for the Baetic Range, –5.79°C km^{-1} for the Iberian Range, and –5.28°C km^{-1} for the CS. The $NSLR_{dmax}$ and $NSLR_{dmin}$ values (see supplementary Figures S1-S2) showed larger daily variability than the $NSLR_{dmean}$, while the median daily zonal values (see supplementary Tables S1-S2) showed steepest lapse rates for the $NSLR_{dmax}$ in the Pyrenees and the Central and the Iberian ranges, and for the $NSLR_{dmin}$ in the Cantabrian and the Baetic ranges.

Figure 5 shows box-and-whisker plots of $NSLR_{dmean}$ for each month and for the various mountain areas, revealing clear differences among them. The Wilcoxon-Mann-Whitney test showed that there were significant differences ($p < 0.05$) among monthly $NSLR_{dmean}$ values for most of the combinations between months in each mountain area (351 of 396 combinations). Except for the summer months in the Central Range, where the $NSLR_{dmean}$ values were very similar to the MELR, the other months showed lapse rates noticeably weaker than –6.5°C km^{-1}. In the Pyrenees and the Central and the Iberian ranges, the steepest monthly $NSLR_{dmean}$ values occurred in summer and spring (May–September), weakening in autumn and winter. In contrast, the steepest monthly $NSLR_{dmean}$ values for the Cantabrian and the Baetic ranges were recorded in the coldest months (i.e., November–February), while decreased in spring and summer. The CS showed the steep NSLR value during each equinoctial seasons (i.e, April–May and October–November), being of lesser magnitude in winter and summer (i.e., December–January and July–August). The Iberian Range recorded the least seasonal variability, and the Central Range the greatest. The winter months were typically more variable

than those in summer. The median monthly NSLR values (Table 2) showed that the two most extreme months for each mountain range were: April (–5.71°C km^{-1}) and December (–4.16°C km^{-1}) for the Pyrenees; February (–6.03°C km^{-1}) and July (–4.02°C km^{-1}) for the Cantabrian Range; June (–6.71°C km^{-1}) and December (–3.92°C km^{-1}) for the Central Range; November (–5.59°C km^{-1}) and July (–3.03°C km^{-1}) for the Baetic Range; and April (–6.28°C km^{-1}) and December (–5.28°C km^{-1}) for the Iberian Range. CS had the steepest median monthly $NSLR_{dmean}$ in April (–5.80°C km^{-1}) and the weakest in July (–4.67°C km^{-1}). A separate analysis of $NSLR_{dmax}$ and $NSLR_{dmin}$ revealed that the seasonality was less marked for $NSLR_{dmin}$, especially for the Cantabrian Range and the CS (see supplementary Figures S3-S4). Median monthly values of $NSLR_{dmax}$ and $NSLR_{dmin}$ were also calculated and can be found in the supplementary Tables S1-S2.

4.2 Synoptic $NSLR_{dmean}$ analysis

The weather type classification revealed that the most frequent CWTs (Fig. 6) were the A (23.4%, 85.8 days yr^{-1}) and C (17.4%, 63.8 days yr^{-1}) aggregated types, followed by the N type (11.1%, 40.6 days yr^{-1}). The less frequent CWTs were the S (3.3%, 12 days yr^{-1}) and the A+ (3.8%, 13.8 days yr^{-1}) types. Summer months were influenced by the N, NE, A and C types, whereas in winter the occurrence of CWTs varied, with the A+ and the W advections being the most frequent ones.

The Wilcoxon-Mann-Whitney test identified significant differences ($p < 0.05$) in $NSLR_{dmean}$ amongst the CWTs for the majority of combinations between CWTs in each mountain area (347 of 396 combinations). Figure 7 shows that the steepest $NSLR_{dmean}$ occurred with the N, NE, and NW weather types for the majority of mountain ranges and the CS. In contrast, the weakest $NSLR_{dmean}$ took place under the A+ and A types,

and southerly advections (S and SE). An exception to this pattern occurred in the Cantabrian Range, where the steepest $NSLR_{dmean}$ corresponded to the SW and W advections. In the case of the Baetic Range the A and A+ types did not reduce the $NSLR_{dmean}$, as occurred for the rest of mountain areas.

The $NSLR_{dmean}$ for each CWTs and regions are shown in Table 2, being the extreme values as follows: the Pyrenees (N –5.75 °C km^{-1}, A+ –3.55 °C km^{-1}); the Cantabrian Range (SW –7.07 °C km^{-1}, SE –3.65 °C km^{-1}); the Central Range (N –6.70 °C km^{-1}, A+ –2.29 °C km^{-1}); the Baetic Range (NW –5.69 °C km^{-1}, A –4.32 °C km^{-1}); the Iberian Range (NE –6.83 °C km^{-1}, S –4.57 °C km^{-1}). CS had the steepest $NSLR_{dmean}$ with the NW type (–6.10 °C km^{-1}) and the weakest with the A+ type (–4.30°C km^{-1}). The variability of $NSLR_{dmean}$ was similar for all CWTs, except for A and A+ situations showing large standard deviations values. The behavior of the $NSLR_{dmax}$ and $NSLR_{dmin}$ (see supplementary Figures S5-S6) was similar, with less variability for the $NSLR_{dmin}$ values. Median values for $NSLR_{dmax}$ and $NSLR_{dmin}$ under the different CWTs were also calculated (see supplementary Tables S1-S2).

4.3 Combined monthly synoptic analysis

Figure 8 shows the differences in $NSLR_{dmean}$ values for all possible combinations of CWTs and months. These values can be considered to be reference values for NSLR, and 132 Monthly–CWTs combinations are being proposed here as reference values for each study area. In the vast majority of cases $NSLR_{dmean}$ values were weaker than the MELR value (–6.5°C km^{-1}). In addition, it was observed that steepest $NSLR_{dmean}$ values tended to occur in spring and early summer months (i.e., April–June), and in autumn (i.e., September–November), associated with northerly CWTs (principally N and NW) and atmospheric instability across CS. On the contrary, the weakest $NSLR_{dmean}$ values

occurred in summer (i.e., June–August) and winter (i.e. December-January), associated with southerly (S) and anticyclonic (A and A+) CWTs, respectively, with stable atmospheric conditions dominating across the CS. In particular, the Cantabrian and the Baetic ranges also exhibited very weak $NSLR_{dmean}$ values under all possible CWTs in summer months. Figure 8 shows the accuracy of the proposed values (at the 95% confidence interval), which was determined from goodness of fit to the model regression and the number of stations involved in the calculation (bolded values in Fig. 8 imply < ±1.0°C km^{-1}). The Central Range was the most difficult region for defining a $NSLR_{dmean}$ value (~ ±1.6°C km^{-1}), with the Baetic Range being the easiest one (~ ±0.9°C km^{-1}). The CS showed a low absolute error (~ ±0.4°C km^{-1}) as a result of the large number of stations and the robustness of the regression models. In terms of uncertainty, the southerly (S, SE) and anticyclones (A, A+) CWTs displayed the largest values while the northerly (N, NW) CWTs showed the lowest ones. Finally, the median $NSLR_{dmax}$ and $NSLR_{dmin}$ values for all possible combinations of CWTs and months were calculated and are provided in the supplementary Figures S7–S8.

4.4 Proposed reference $NSLR_{dmean}$ values and validation

Table 2 shows our proposal of Zonal, Monthly, and CWTs reference $NSLR_{dmean}$ values (Table 2) for CS and the major mountain ranges.

The accuracy of the proposed $NSLR_{dmean}$ values is shown in Table 3 for each study area and season. The fixed MELR and Zonal NSLR displayed the largest errors in all study areas, while the hybrid Monthly–CWTs showed the smallest errors. For the Cantabrian and the Iberian ranges the proposed monthly values were associated with larger errors than the proposed CWTs values, which contrasts to the findings for the Central and the Baetic ranges. Both Monthly and CWTs values were similar for the Pyrenees, which

showed the smallest errors, whereas the largest errors were found for the Central and the Iberian ranges. Seasonally, the MAE values revealed marked differences, which were largest for the fixed lapse rates (MELR and Zonal).

5. Discussion

Near-surface air temperature lapse rates based on records of daily averages ($NSLR_{dmean}$) were analyzed for the major mountain ranges in continental Spain. Our results found spatial changes in $NSLR_{dmean}$ as a function of the month of the year and synoptic conditions (i.e., CWTs). The weather station network used in this study included a large number of weather stations at elevation ranges from 0 to 1500 m a.s.l, but with few number of stations above 1500 m a.s.l. The lack of high elevation stations is a common problem in many previous studies (e.g., Blöschl, 1991; Rolland, 2003; Benavides et al., 2007; Du et al., 2017). Thus, our results are robust for interpolating air temperatures at low and medium elevations, whereas lapse rate values for high elevation mountain areas have to be interpreted with caution. For instance, low humidity and katabatic winds could markedly affect the slope of NSLRs (Heynen et al., 2016) in areas of complex topography at high elevations. Therefore, the increase in the density of high-elevation stations would help to overcome this limitation over mountainous areas.

Previous studies have reported a strong inverse relationship between elevation and mean annual air temperature (Barry and Chorley, 1987), highlighting the strength of our methodological approach to calculate NSLR based on changes in elevation. Overall, we found that the $NSLR_{dmean}$ (–5.28°C km^{-1}) was weaker than the standard MELR value (–6.5°C km^{-1}), which is widely used in the scientific literature; this suggests that the use of the MELR to interpolate near-surface air temperatures may lead to large inaccuracies, particularly over high-elevation mountain ranges. Additionally, we found large

differences in $NSLR_{dmean}$ values among the studied mountain ranges (the Pyrenees: –5.17°C km^{-1}; the Cantabrian Range: –5.22°C km^{-1}; the Central Range: –5.78°C km^{-1}; the Baetic Range: –4.83°C km^{-1}; and the Iberian Range: –5.79°C km^{-1}), and also in the accuracy (standard deviation) of the estimated averages (the Pyrenees: 1.40°C km^{-1}; the Cantabrian Range: 1.73°C km^{-1}; the Central Range: 2.06°C km^{-1}; the Baetic Range: 1.53°C km^{-1}; the Iberian Range: 1.64°C km^{-1}; and CS: 1.15°C km^{-1}). Differences in the slope of $NSLR_{dmean}$ and its variability might be due to the degree of continentality and its effect on prevailing atmospheric conditions for each mountain region. This phenomenon has been previously reported for polar (Marshall et al., 2007) and Chinese (Fang and Yoda, 1988; Li et al., 2013) areas; in the latter case especially for mountain ranges receiving less radiation in the northern slopes (Lookingbill and Urban, 2003), as quantified by McCutchan et al. (1986). Thus, dry continental conditions (e.g., in the Central and the Iberian ranges) resulted in the highest Zonal $NSLR_{dmean}$ values, whereas the increased moisture and exposure to oceanic winds and cloudiness in lowland areas might lead to a reduced Zonal $NSLR_{dmean}$, as occurred for the Baetic and the Cantabrian ranges (Capel Molina, 2000). The Pyrenees may present an intermediate pattern, with oceanic/sea influences in the westernmost and easternmost areas, and continental influences (albeit prone to severe winter thermal inversions) in the central area. Regional topography is a key element in understanding the behavior of near-surface air temperature lapse rates. Beyond the mean annual $NSLR_{dmean}$ values, it is imperative to consider their temporal variability (Bolstad et al., 1998; Minder et al., 2010). Our results showed a marked seasonality for the entire CS, and also for each of the 5 mountain areas analyzed. The results for CS showed that the steepest $NSLR_{dmean}$ occurred in the equinoctial seasons (autumn and spring), and decreased in winter and summer. The cold

season is typically found to be associated with weak $NSLR_{dmean}$ values, because of the prevalence of stable atmospheric conditions and the development of thermal inversions (Blöschl, 1991; Bolstad et al., 1998; Tang and Fang, 2006; Marshall et al., 2007; Blandford et al., 2008; Gardner et al., 2009; Kattel et al., 2013). Our results for thermal inversions are consistent with the findings at local scales reported for the Pyrenees by Pagès and Miró (2010) and Puigdefábregas (1969), who identified a marked weakening of NSLRs under anticyclonic conditions. In the majority of the analyzed mountain areas the steepest $NSLR_{dmean}$ values were found in spring, which is consistent with previous studies in the Alps (Dumas, 2013; Kirchner et al., 2013), the Pennines (Pepin, 2001), and the Rocky Mountains (Pepin and Seidel, 2005; Blandford et al., 2008). This behavior might be due to the persistence of snow cover at highest stations in winter and, occasionally, in spring due to heat exchange and albedo as previously proposed by Rolland (2003), Pepin and Kidd (2006) or Pagès et al. (2017). In the mountain area nearest to the ocean (the Cantabrian Range), the weakest $NSLR_{dmean}$ occurred in summer. This might be associated with the local synoptic effects in summer months, in which northerly flows result in low stratiform clouds along the coastal fringe. This also occurred for the Baetic Range, but over this mountain are this could be related to the heat in the warm inland valleys, beyond the coastal and temperate locations. Generally, the variability of $NSLR_{dmean}$ values was great in winter for all mountain ranges because the occurrence of both stable and unstable atmospheric circulations.

We also found that weather types have a significant impact on the $NSLR_{dmean}$. This finding, particularly for the Pyrenees and the Central Range, is consistent with previous studies showing that the most stable weather types (i.e., anticyclonic situations) are associated with the lowest $NSLR_{dmean}$ values, mainly because of the high occurrence of

thermal inversions (Pepin and Kidd, 2006; Marshall et al., 2007), whereas the highest $NSLR_{dmean}$ values occur under unstable synoptic conditions (Kirchner et al., 2013) with cold air in the mid- to high-layers of the troposphere. We also found extreme high pressures (A+) were associated with very weak $NSLR_{dmean}$ values. In contrast, northerly weather types showed the steepest $NSLR_{dmean}$ values, consistent with previous studies in Europe (Pepin, 2001; Holden and Rose, 2011), and Antarctica (southern hemisphere) (Braun and Hock, 2004). Northerly situations bring cold air masses over the CS, in particular at high mountain elevations, resulting in increased $NSLR_{dmean}$ values. As an exception, the steepest $NSLR_{dmean}$ values occur under SW flows in the Cantabrian range, where the Foehn effect causes an overheating along the coast. Other atmospheric parameters such as wind, humidity, and atmospheric pressure can also affect the $NSLR_{dmean}$ (Blandford et al., 2008; Dumas, 2013; Li et al., 2013; Immerzeel et al., 2014), and are directly related to the prevailing synoptic conditions. Future studies will be directed towards improving our understanding of the effect of these atmospheric parameters on the $NSLR_{dmean}$. However, the complexity of CS suggests that the relative impact of each atmospheric parameter may vary spatially.

Here we also proposed reference $NSLR_{dmean}$ values as a function of the time of the year, circulation weather types (CWTs) and study area. For instance, the combinations of months and CWTs revealed that the effects of the northwest CWT is not the same in January and August. In addition, the analysis of confidence intervals enabled the estimation of uncertainty. In some study areas the seasonality tended to have a large effect (e.g. the Baetic Range), while in others the $NSLR_{dmean}$ values were more influenced by synoptic conditions (e.g., the Cantabrian Range). The results and reference values obtained in this study are not necessarily representative for other

regions, as there was large spatial, seasonal, and synoptic variability, and local factors can play a key role (Nunez and Calhoun, 1986; Pepin and Seidel, 2005; Marshall et al., 2007). However, the approach presented can serve as guide to improving estimates of $NSLR_{dmean}$ in other regions.

Validation of the reference NSLR results showed that the MAE decreased for Monthly, CWTs and hybrid Monthly–CWTs. In this context, Marshall et al. (2007) and Minder et al. (2010) not recommended the use of fixed lapse rates. The study areas showing large variability in $NSLR_{dmean}$, corresponded to regions with high MAE. In this regard seasonal differences were marked, especially between winter (i.e., December–February) and equinoctial seasons (i.e., March–June; September–November). This is because synoptic conditions can usually change from one day to the other in winter, while atmospheric instability tends to dominate in spring and autumn. There were no large differences between the proposed Monthly and CWTs NSLRs in the validation process. The best approach was the proposed hybrid Monthly-CWTs NSLRs. In cases where the proposed reference CWTs values had lower MAEs than monthly values, synoptic conditions better explained the near-surface air temperature lapse rates than seasonal ones, and vice versa.

In any case, MAE values were large (until ~1.8°C), which indicates that although the estimates of air temperature took account of latitude, longitude, distance to the sea, and topographic position, others factors could also influence the spatial distribution of near-surface air temperatures (Lookingbill and Urban, 2003). Mountainous areas represent unique environments for detecting climate change and its impacts. Modeling plays a key role in the prediction and amelioration of future climate scenarios, facilitating response actions and preparing the society for change. Improvements in determining near-surface

temperature lapse rates will help reduce uncertainties in any modeling involving the use of climatic variables, such as hydrological models and mass balance snow and glacier simulations.

6. Conclusion

The major findings of the spatio-temporal analysis of near-surface air temperature lapse rates for continental Spain and its five most important mountain regions for December 1979 to August 2015 are:

- Near-surface air temperature lapse rates based on daily mean air temperatures ($NSLR_{dmean}$) were weaker than the standard Mean Environmental Lapse Rate (MELR) value of –6.5°C km^{-1}, which is commonly used for interpolating and extrapolating air temperatures. Moreover, the $NSLR_{dmean}$ varied spatially and seasonally, and depended on the prevailing synoptic conditions. All median $NSLR_{dmean}$ were weaker than –6.5°C km^{-1}, and ranged from –4.83°C km^{-1} for the Baetic Range to –5.79°C km^{-1} for the Iberian Range. The median $NSLR_{dmean}$ was –5.28°C km^{-1} for CS. The steepest $NSLR_{dmean}$ values occurred in spring and autumn for CS, in spring and early summer for the Pyrenees and the Central and Iberian ranges, and in autumn and early winter for the Cantabrian and the Baetic ranges.
- Anticyclonic and southerly circulation weather types (CWTs) favored thermal inversions and the weakening of the $NSLR_{dmean}$. Northerly weather types enhanced steep NSLRs. The same response of $NSLR_{dmean}$ values to CWTs was found for all study areas, except for the weakening effect of high pressure circulations on $NSLR_{dmean}$ values which was less pronounced in the mountain areas close to oceanic air masses (e.g., the Baetic and the Cantabrian ranges).

549 - Fixed lapse rates such as the MELR and Zonal lapse rates are not recommended
550 because of the large residuals found. Therefore, we strongly encourage the use
551 of well-defined Monthly–CWTs lapse rates for future applications.

552 **7. Acknowledgements**

553 This study is funded by the research projects CGL2014-52599-P "*Estudio del manto de*
554 *nieve en la montaña española y su respuesta a la variabilidad y cambio climatico*" and
555 CLIMPY "*Characterization of the evolution of climate and provision of information for*
556 *adaptation in the Pyrenees"* (FEDER-POCTEFA). We thank the Spanish
557 Meteorological Agency (AEMET) for the air temperature data used in this study. The
558 first author and M. T-B are granted with a pre-doctoral FPU grant (Spanish Ministry of
559 Education, Culture and Sports), and C. A-M has received funding from the European
560 Union's Horizon 2020 research and innovation programme under the Marie
561 Skłodowska-Curie grant agreement No. STILLING project-703733. The authors thank
562 all colleagues who helped in the development of the experiments, and wish to
563 acknowledge the three anonymous reviewers for their detailed and helpful comments on
564 the original manuscript.

565 **REFERENCES**

566 AEMET (2011). *Atlas Climático Ibérico*. Agencia Estatal de Meteorología - Ministerio de Medio
567 Ambiente y Medio Rural y Marino and Instituto de Meteorología de Portugal (eds). 1st ed., Closas-
568 Orcoyen S. L., Madrid.

569 Barringer, J. R. F. (1989). A variable lapse rate snowline model for the Remarkables, Central Otago, New
570 Zealand. Journal of Hydrology (N.Z.), 28(1) 32–46.

571 Barry, R. G. (1992). *Mountain weather and Climate*. 2nd ed., Psychology Press.

572 Barry, R. G. (2001). Mountain Climate Change and Cryospheric Responses: A review. *In* Berger, T. et al.

(ed.) Mountain of the world. Proceedings of the World Mountain Symposium. Bern, Switzerland.

Barry, R. G. and Chorley, R. J. (1987). *Atmosphere, Weather and Climate*. 1st ed.

Basnett, T. A. and Parker, D. E. (1997). Development of the global mean sea level pressure data set GMSLP2. *In* Office, H. C.-M. (ed.) Climatic Research Technical Note. Bracknell.

Benavides, R., Montes, F., Rubio, A. and Osoro, K. (2007). Geostatistical modelling of air temperature in a mountainous region of Northern Spain. Agricultural and Forest Meteorology, 146(3) 173–188.

Blandford, T. R., Humes, K. S., Harshburger, B. J., Moore, B. C., Walden, V. P., Ye, H., Blandford, T. R., Humes, K. S., Harshburger, B. J., Moore, B. C., Walden, V. P. and Ye, H. (2008). Seasonal and Synoptic Variations in Near-Surface Air Temperature Lapse Rates in a Mountainous Basin. Journal of Applied Meteorology and Climatology, 47(1) 249–261.

Blöschl, G. (1991). The influence of Uncertainty in Air Temperature and Albedo on Snowmelt. Hydrology Research, 22(2) 95–108.

Bolstad, P. V., Swift, L., Collins, F. and Régnière, J. (1998). Measured and predicted air temperatures at basin to regional scales in the southern Appalachian mountains. Agricultural and Forest Meteorology, 91(3–4) 161–176.

Braun, M. and Hock, R. (2004). Spatially distributed surface energy balance and ablation modelling on the ice cap of King George Island (Antarctica). Global and Planetary Change, 42(1) 45–58.

Buisan, S. T., Azorin-Molina, C. and Jimenez, Y. (2015). Impact of two different sized Stevenson screens on air temperature measurements. International Journal of Climatology, 35(14) 4408–4416.

Buisan, S. T., Saz, M. A. and López-Moreno, J. I. (2015). Spatial and temporal variability of winter snow and precipitation days in the western and central Spanish Pyrenees. International Journal of Climatology, 35(2) 259–274.

Capel Molina, J. J. (2000). *El clima de la Península Ibérica*. Ariel.

Du, M., Liu, J., Zhang, X., Li, Y. and Tang, Y. (2010). Changes of spatial patterns of surface-air-temperature on the Tibetan Plateau. Latest Trends on Theoretical and Applied Mechanics, Fluid Mechanics and Heat & Mass Transfer.

599 Du, M., Zhang, M., Wang, S., Zhu, X. and Che, Y. (2017). Near-surface air temperature lapse rates in
600 Xinjiang, northwestern China. Theoretical and Applied Climatology, January, 1–14.

601 Dumas, M. D. (2013). Changes in temperature and temperature gradients in the French Northern Alps
602 during the last century. Theoretical and Applied Climatology. Springer Vienna, 111(1–2) 223–233.

603 Durre, I., Menne, M. J., Gleason, B. E., Houston, T. G., Vose, R. S., Durre, I., Menne, M. J., Gleason, B.
604 E., Houston, T. G. and Vose, R. S. (2010). Comprehensive Automated Quality Assurance of Daily
605 Surface Observations. Journal of Applied Meteorology and Climatology, 49(8) 1615–1633.

606 Fang, J.-Y. and Yoda, K. (1988). Climate and vegetation in China (I). Changes in the altitudinal lapse rate
607 of temperature and distribution of sea level temperature. Ecological Research, 3(1) 37–51.

608 Farr, T. G., Rosen, P. A., Caro, E., Crippen, R., Duren, R., Hensley, S., Kobrick, M., Paller, M.,
609 Rodríguez, E., Roth, L., Seal, D., Shaffer, S., Shimada, J., Umland, J., Werner, M., Oskin, M., Burbank,
610 D. and Alsdorf, D. (2007). The Shuttle Radar Topography Mission. Reviews of Geophysics, 45(2)
611 RG2004.

612 García-Herrera, R., Hernández, E., Barriopedro, D., Paredes, D., Trigo, R. M., Trigo, I. F. and Mendes,
613 M. A. (2007). The Outstanding 2004/05 Drought in the Iberian Peninsula: Associated Atmospheric
614 Circulation. Journal of Hydrometeorology, 8(3) 483–498.

615 García-Ruiz, J. M., López-Moreno, J. I., Vicente-Serrano, S. M., Lasanta–Martínez, T. and Beguería, S.
616 (2011). Mediterranean water resources in a global change scenario. Earth-Science Reviews. Elsevier,
617 105(3–4) 121–139.

618 Gardner, A. S., Sharp, M. J., Koerner, R. M., Labine, C., Boon, S., Marshall, S. J., Burgess, D. O. and
619 Lewis, D. (2009). Near-Surface Temperature Lapse Rates over Arctic Glaciers and Their Implications for
620 Temperature Downscaling. Journal of Climate, 22(16) 4281–4298.

621 Goodess, C. M. and Palutikof, J. P. (1998). Development of daily rainfall scenarios for southeast Spain
622 using a circulation - type approach to downscaling. International Journal of Climatology, 10 1051–1083.

623 Hanna, E., Huybrechts, P., Janssens, I., Cappelen, J., Steffen, K. and Stephens, A. (2005). Runoff and
624 mass balance of the Greenland ice sheet: 1958–2003. Journal of Geophysical Research, 110(D13)
625 D13108.

626 Harlow, R. C., Burke, E. J., Scott, R. L., Shuttleworth, W. J., Brown, C. M. and Petti, J. R. (2004).
627 Research Note:Derivation of temperature lapse rates in semi-arid south-eastern Arizona. Hydrology and
628 Earth System Sciences, 8(6) 1179–1185.

629 Heynen, M., Miles, E., Ragettli, S., Buri, P., Immerzeel, W. W. and Pellicciotti, F. (2016). Air
630 temperature variability in a high-elevation Himalayan catchment. Annals of Glaciology, 57(71) 212–222.

631 Holden, J. and Rose, R. (2011). Temperature and surface lapse rate change: a study of the UK's longest
632 upland instrumental record. International Journal of Climatology, 31(6) 907–919.

633 Immerzeel, W. W., Petersen, L., Ragettli, S. and Pellicciotti, F. (2014). The importance of observed
634 gradients of air temperature and precipitation for modeling runoff from a glacierized watershed in the
635 Nepalese Himalayas. Water Resources Research, 50(3) 2212–2226.

636 Jenkinson, A. F. and Collison, P. (1977). An initial climatology of Wales over the North Sea. *In* Synoptic
637 Climatology Branch memorandum, 62.

638 Kattel, D. B., Yao, T., Yang, K., Tian, L., Yang, G. and Joswiak, D. (2013). Temperature lapse rate in
639 complex mountain terrain on the southern slope of the central Himalayas. Theoretical and Applied
640 Climatology, 113(3–4) 671–682.

641 Kirchner, M., Faus-Kessler, T., Jakobi, G., Leuchner, M., Ries, L., Scheel, H.-E. and Suppan, P. (2013).
642 Altitudinal temperature lapse rates in an Alpine valley: trends and the influence of season and weather
643 patterns. International Journal of Climatology. John Wiley & Sons, Ltd., 33(3) 539–555.

644 Kunkel, K. E. (1989). Simple Procedures for Extrapolation of Humidity Variables in the Mountainous
645 Western United States. Journal of Climate, 2(7) 656–670.

646 Lamb, H. H. (1972). British Isles weather types and a register of daily sequence of circulation patterns,
647 1861 - 1971. Geophysical Memoires, 116.

648 Li, X., Wang, L., Chen, D., Yang, K., Xue, B. and Sun, L. (2013). Near-surface air temperature lapse
649 rates in the mainland China during 1962-2011. Journal of Geophysical Research: Atmospheres, 118(14)
650 7505–7515.

651 Lookingbill, T. R. and Urban, D. L. (2003). Spatial estimation of air temperature differences for
652 landscape-scale studies in montane environments. Agricultural and Forest Meteorology, 114(3) 141–151.

López-Moreno, J. I. and Vicente-Serrano, S. M. (2007). Atmospheric circulation influence on the interannual variability of snow pack in the Spanish Pyrenees during the second half of the 20th century. Hydrology Research, 38(1) 33–44.

Lundquist, J. D. and Cayan, D. R. (2007). Surface temperature patterns in complex terrain: Daily variations and long-term change in the central Sierra Nevada, California. Journal of Geophysical Research, 112(D11) D11124.

Marsh, C. (2009). Application and comparison of high resolution radiation models in complex terrain. Geography, 490(2).

Marshall, S. J., Sharp, M. J., Burgess, D. O. and Anslow, F. S. (2007). Near-surface-temperature lapse rates on the Prince of Wales Icefield, Ellesmere Island, Canada: implications for regional downscaling of temperature. International Journal of Climatology, 27(3) 385–398.

Martinec, J., Rango, A. and Major, E. (1983). The Snowmelt-Runoff Model (SRM) user's manual.

McCutchan, M. H. and Fox, D. G. (1986). Effect of Elevation and Aspect on Wind, Temperature and Humidity. Journal of Climate and Applied Meteorology, 25(12) 1996–2013.

Minder, J. R., Mote, P. W. and Lundquist, J. D. (2010). Surface temperature lapse rates over complex terrain: Lessons from the Cascade Mountains. Journal of Geophysical Research, 115(D14) D14122.

Miró, J. R., Peña, J. C., Pepin, N., Sairouni, A. and Aran, M. (2017). Key features of cold-air pool episodes in the northeast of the Iberian Peninsula (Cerdanya, eastern Pyrenees). International Journal of Climatology. John Wiley & Sons, Ltd, August.

Nigrelli, G., Fratianni, S., Zampollo, A., Turconi, L. and Chiarle, M. (2017). The altitudinal temperature lapse rates applied to high elevation rockfalls studies in the Western European Alps. Theoretical and Applied Climatology, February, 1–13.

Nunez, M. and Calhoun, E. A. (1986). A note on air temperature lapse rates on Mount Wellington, Tasmania. Papers and Proceedings of the Royal Society of Tasmania Tasmania. Pap. Proc. R. Soc. Tasm, 12012(120) 11–15.

Pagès, M. and Miró, J. R. (2010). Determining temperature lapse rates over mountain slopes using vertically weighted regression: a case study from the Pyrenees. Meteorological Applications, 17(1) 53–

63.

Pagès, M., Pepin, N. and Miró, J. R. (2017). Measurement and modelling of temperature cold pools in the Cerdanya valley (Pyrenees), Spain. Meteorological Applications. John Wiley & Sons, Ltd, 24(2) 290–302.

Pepin, N. (2001). Lapse rate changes in northern England. Theoretical and Applied Climatology, 68(1–2) 1–16.

Pepin, N., Benham, D. and Taylor, K. (1999). Modeling Lapse Rates in the Maritime Uplands of Northern England: Implications for Climate Change. Arctic, Antarctic, and Alpine Research, 31(2) 151–164.

Pepin, N. C., Daly, C. and Lundquist, J. (2011). The influence of surface versus free-air decoupling on temperature trend patterns in the western United States. Journal of Geophysical Research, 116(D10) D10109.

Pepin, N. C. and Seidel, D. J. (2005). A global comparison of surface and free-air temperatures at high elevations. Journal of Geophysical Research, 110(D3) D03104.

Pepin, N. and Kidd, D. (2006). Spatial temperature variation in the Eastern Pyrenees. Weather, 61(11) 300–310.

Pepin, N. and Losleben, M. (2002). Climate change in the Colorado Rocky Mountains: free air versus surface temperature trends. International Journal of Climatology, 22(3) 311–329.

Puigdefábregas, J. (1969). Avance para un estudio climatologico del alto aragon. Pirineos 76–80.

Rasilla Álvarez, D. F., García-Codrón, J. C. and Garmendia Pedraja, C. (2002). Los temporales de viento: propuesta metodológica para el análisis de un fenómeno infravalorado. *In* Reunión Nacional de Climatología, pp. 129–136.

Rodríguez-Puebla, C., Encinas, A. H., Nieto, S. and Garmendia, J. (1998). Spatial and temporal patterns of annual precipitation variability over the Iberian Peninsula. International Journal of Climatology, 18(3) 299–316.

Rolland, C. (2003). Spatial and Seasonal Variations of Air Temperature Lapse Rates in Alpine Regions.

706 Journal of Climate, 16(7) 1032–1046.

707 Running, S. W., Nemani, R. R. and Hungerford, R. D. (1987). Extrapolation of synoptic meteorological
708 data in mountainous terrain and its use for simulating forest evapotranspiration and photosynthesis.
709 Canadian Journal of Forest Research, 17(6) 472–483.

710 Spellman, G. (2000). The application of an objective weather-typing system to the Iberian peninsula.
711 Weather, 55(10) 375–385.

712 Tang, Z. and Fang, J. (2006). Temperature variation along the northern and southern slopes of Mt. Taibai,
713 China. Agricultural and Forest Meteorology, 139(3) 200–207.

714 Tomás-Burguera, M., Jiménez Castañeda, A., Luna Rico, M. Y., Morata, A., Vicente Serrano, S.,
715 González-Hidalgo, J. C. and Beguería, S. (2016). Control de calidad de siete variables del banco nacional
716 de datos de AEMET. *In* Asociación Española de Climatología Congreso (10. 2016. Alicante) (ed.) X
717 Congreso Internacional AEC: Clima, sociedad, riesgos y ordenación del territorio. Alicante, Spain, pp.
718 407–415.

719 Tomás, C., de Pablo, F. and Rivas Soriano, L. (2004). Circulation weather types and cloud-to-ground
720 flash density over the Iberian Peninsula. International Journal of Climatology, 24(1) 109–123.

721 Trigo, R. M. and Dacamara, C. C. (2000). Circulation Weather Types and their influence on the
722 Precipitation regime in Portugal. International Journal of Climatology, 20 1559–1581.

723 USDMA (2000). *Vector Map Level 0 (VMAP0)*. [Online] [Accessed on 13th July 2017]
724 https://www.lib.msu.edu/branches/map/findingaids/VMAP0/.

725 Vicente-Serrano, S. M. (2007). Evaluating the Impact of Drought Using Remote Sensing in a
726 Mediterranean, Semi-arid Region. Natural Hazards. Springer Netherlands, 40(1) 173–208.

727 Whiteman, C. D., Bian, X., Zhong, S., Whiteman, C. D., Bian, X. and Zhong, S. (1999). Wintertime
728 Evolution of the Temperature Inversion in the Colorado Plateau Basin. Journal of Applied Meteorology,
729 38(8) 1103–1117.

730 Whiteman, C. D., Pospichal, B., Eisenbach, S., Weihs, P., Clements, C. B., Steinacker, R., Mursch-
731 Radlgruber, E. and Dorninger, M. (2004). Inversion Breakup in Small Rocky Mountain and Alpine
732 Basins. Journal of Applied Meteorology, 43(8) 1069–1082.

733 Wilcoxon, F. (1945). Individual Comparisons by Ranking Methods. Biometrics Bulletin. International
734 Biometric Society, 1(6) 80.

735 WMO (2008). *Guide to Meteorological Instruments and Methods of Observation*. 1st ed., Geneva,
736 Switzerland.

737

738

739

740

741

742

743

744 **FIGURES**

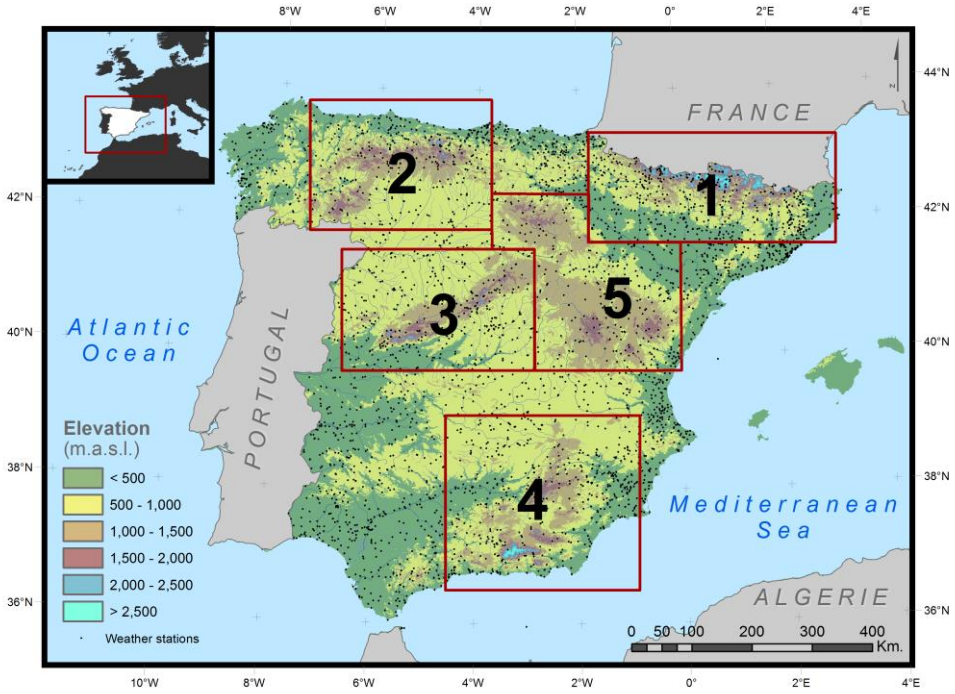

745

746 **Figure 1. Terrain map of continental Spain (CS) showing the location of weather stations (black dots) used in**
747 **this study; red boxes and numbers show to the mountain areas analyzed: (1) Pyrenees; (2) Cantabrian Range;**
748 **(3) Central Range; (4) Baetic Range; and (5) Iberian Range.**

749

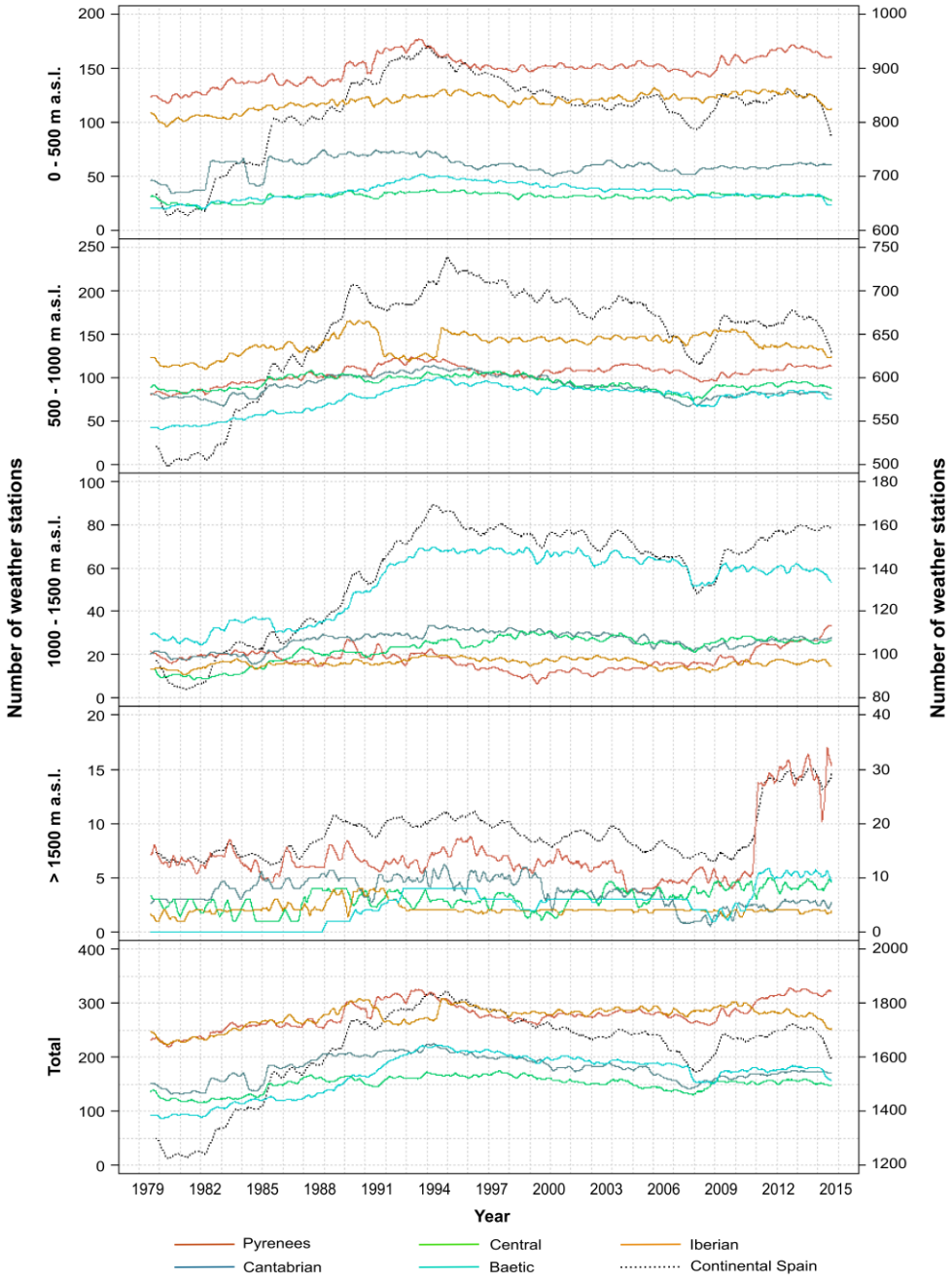

750

751 **Figure 2. Number of weather stations having daily air temperature data as a function of elevation range.**
752 **Mountain ranges were represented on the left y axis. Total amount of Continental Spain was represented on**
753 **the right y axis.**

754

755

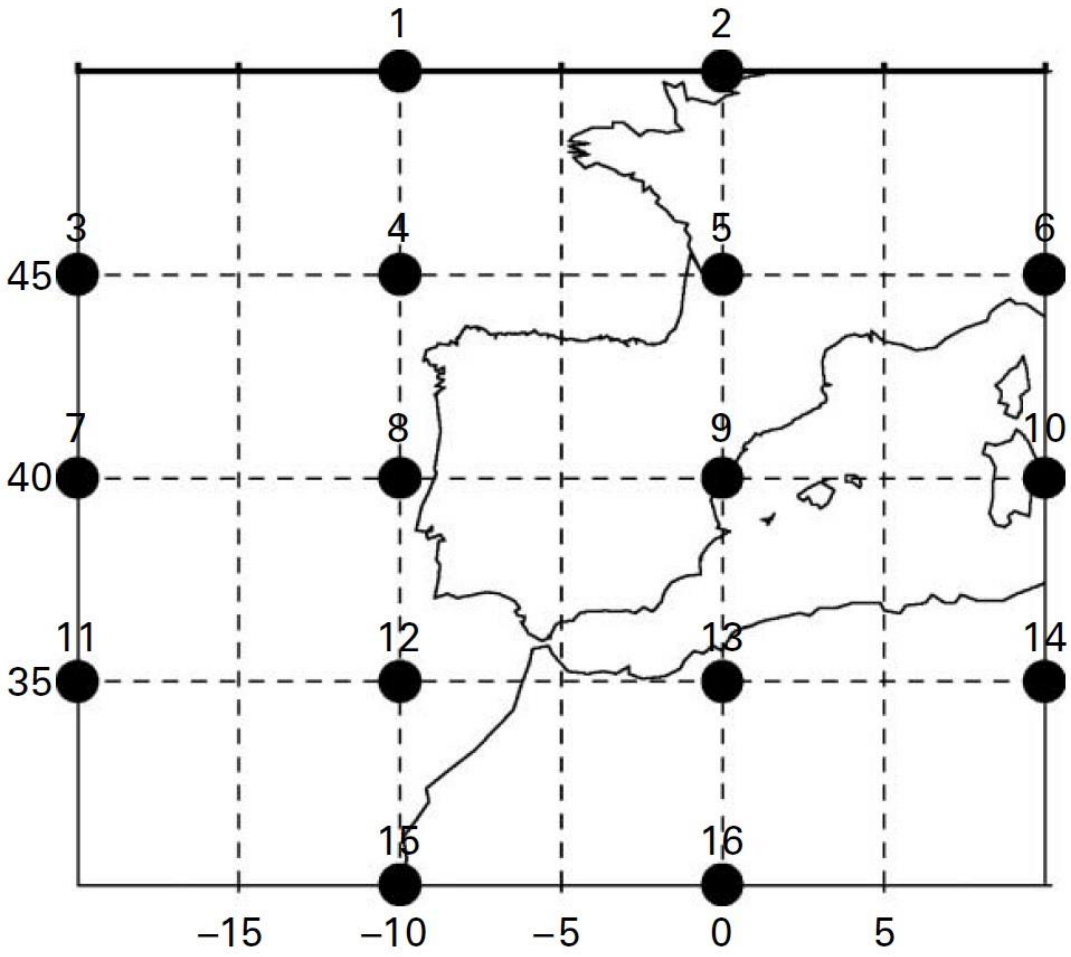

Figure 3. Grid of sea level pressure (SLP) points used to classify the Circulation Weather Types (CWTs) over the Iberian Peninsula.

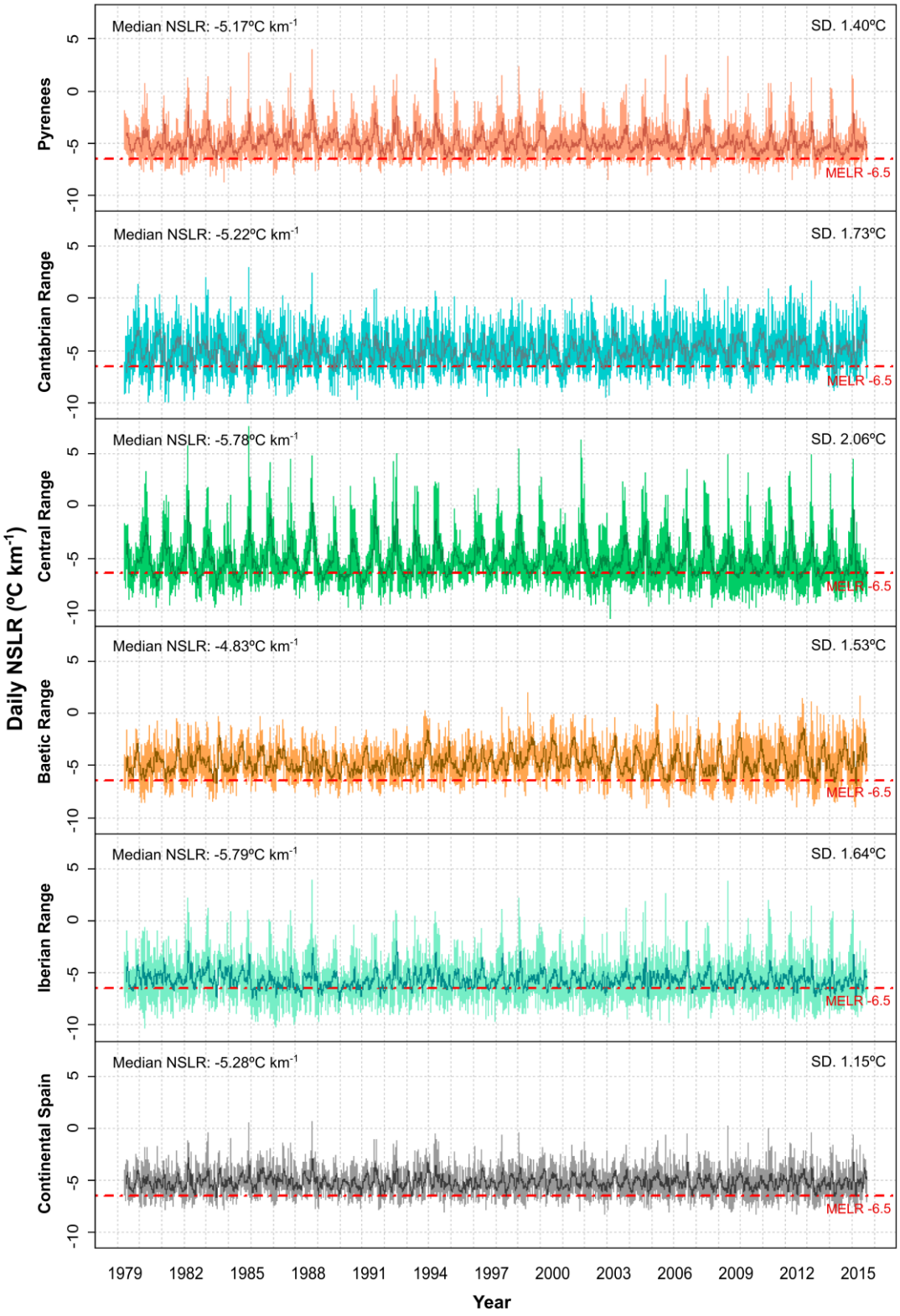

Figure 4. Daily mean near-surface air temperature lapse rate ($NSLR_{dmean}$ °C km^{-1}). Dark colored lines show the 30-day running average. Dashed red lines show the standard and fixed mean environmental lapse rate (MELR) of –6.5°C km^{-1}. SD: standard deviation.

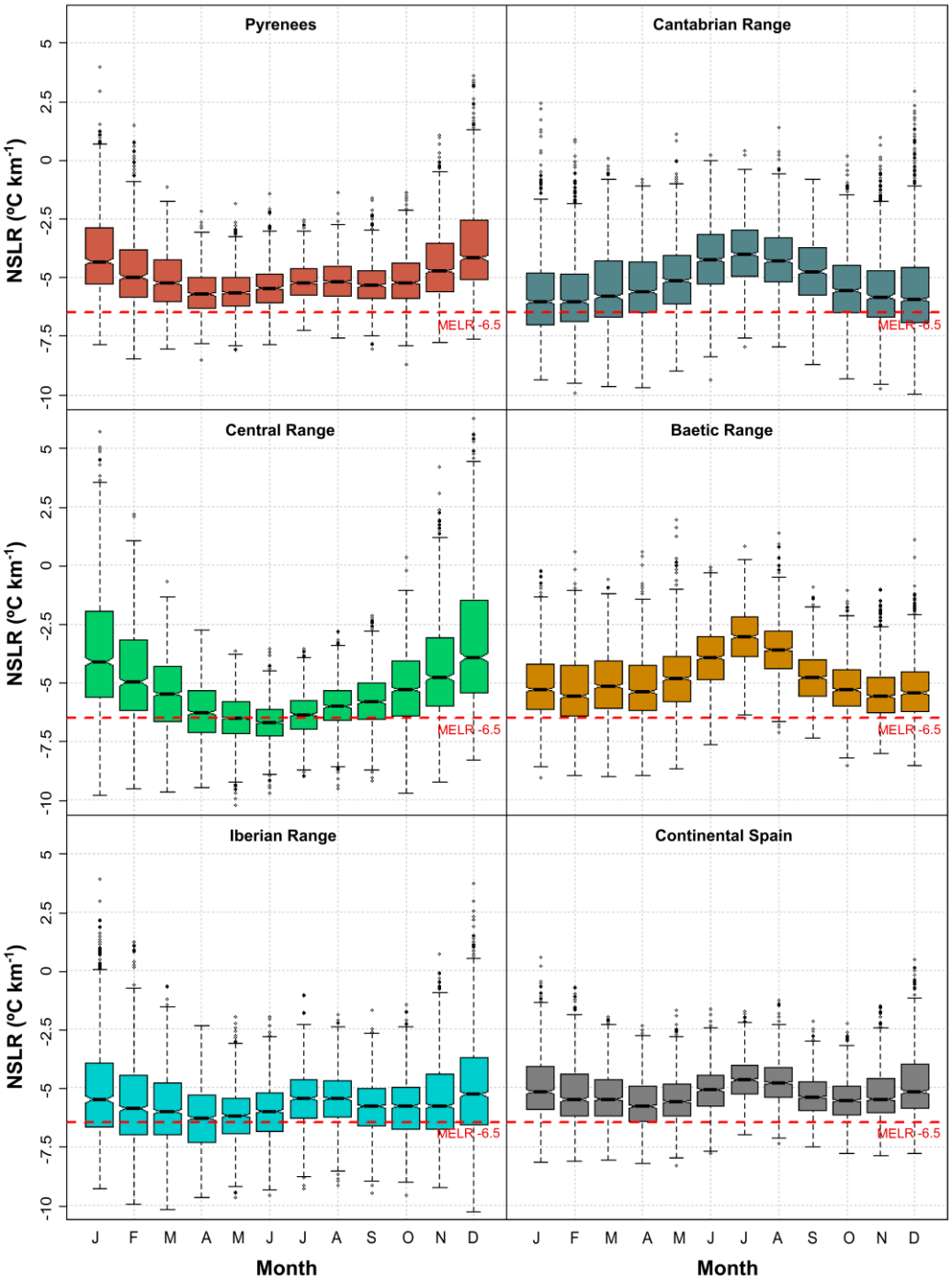

Figure 5. Monthly box-and-whisker plots of daily mean near-surface air temperature lapse rate ($NSLR_{dmean}$: °C km^{-1}) for the five mountain ranges and the entire CS. Dashed red lines show the standard and fixed mean environmental lapse rate (MELR) of –6.5°C km^{-1}. The median (black line), 25th and 75th percentile ranges (boxes), 75th + 1.5IQR (upper whisker), 25th - 1.5IQR (bottom whisker), and the extreme values (> 75th + 1.5IQR and < 25th – 1.5IQR) are represented.

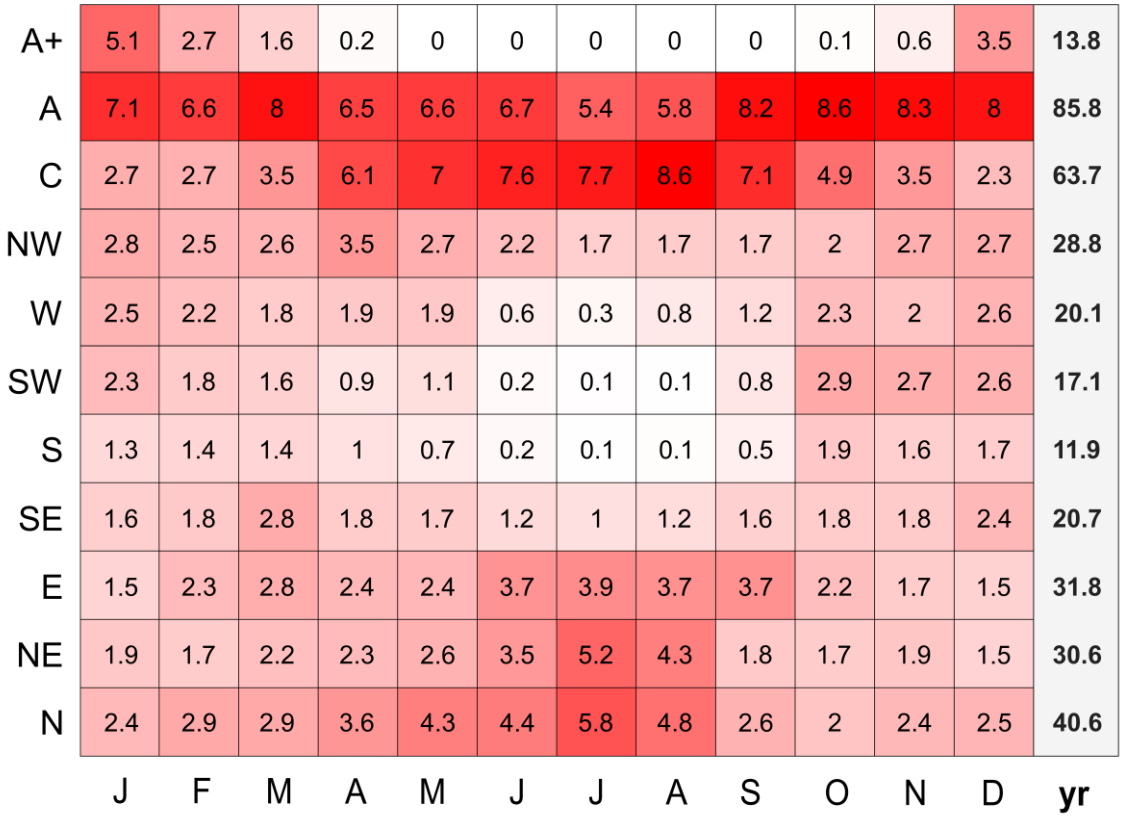

Figure 6. Frequency (in number of days per year; days yr^{-1}) of synthetized circulation weather types (CWTs), based on Jenkinson and Collison (1977) classification for December 1979–August 2015.

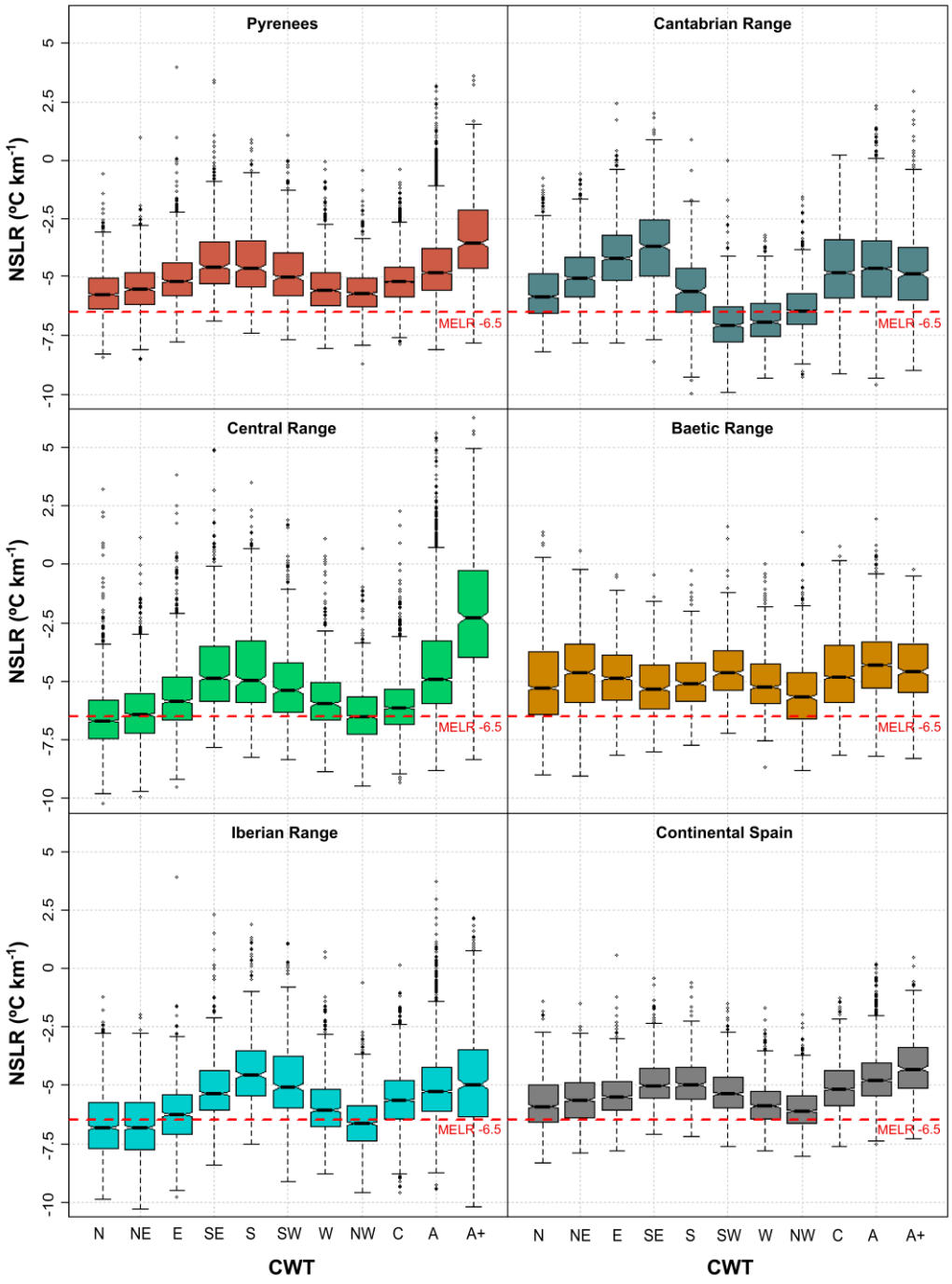

773

774 **Figure 7. Variability in the daily mean near-surface air temperature lapse rate ($NSLR_{dmean}$: °C km^{-1}) for**
775 **various synthetized circulation weather types (CWTs). Dashed red lines show the standard and fixed mean**
776 **environmental lapse rate (MELR) of –6.5°C km^{-1}. The median (black line), the 25th and 75th percentile range**
777 **(boxes), 75^{th} + 1.5IQR (upper whisker), 25^{th} - 1.5IQR (bottom whisker), and the extreme values (> 75^{th} +**
778 **1.5IQR and < 25^{th} – 1.5IQR) are represented.**

779

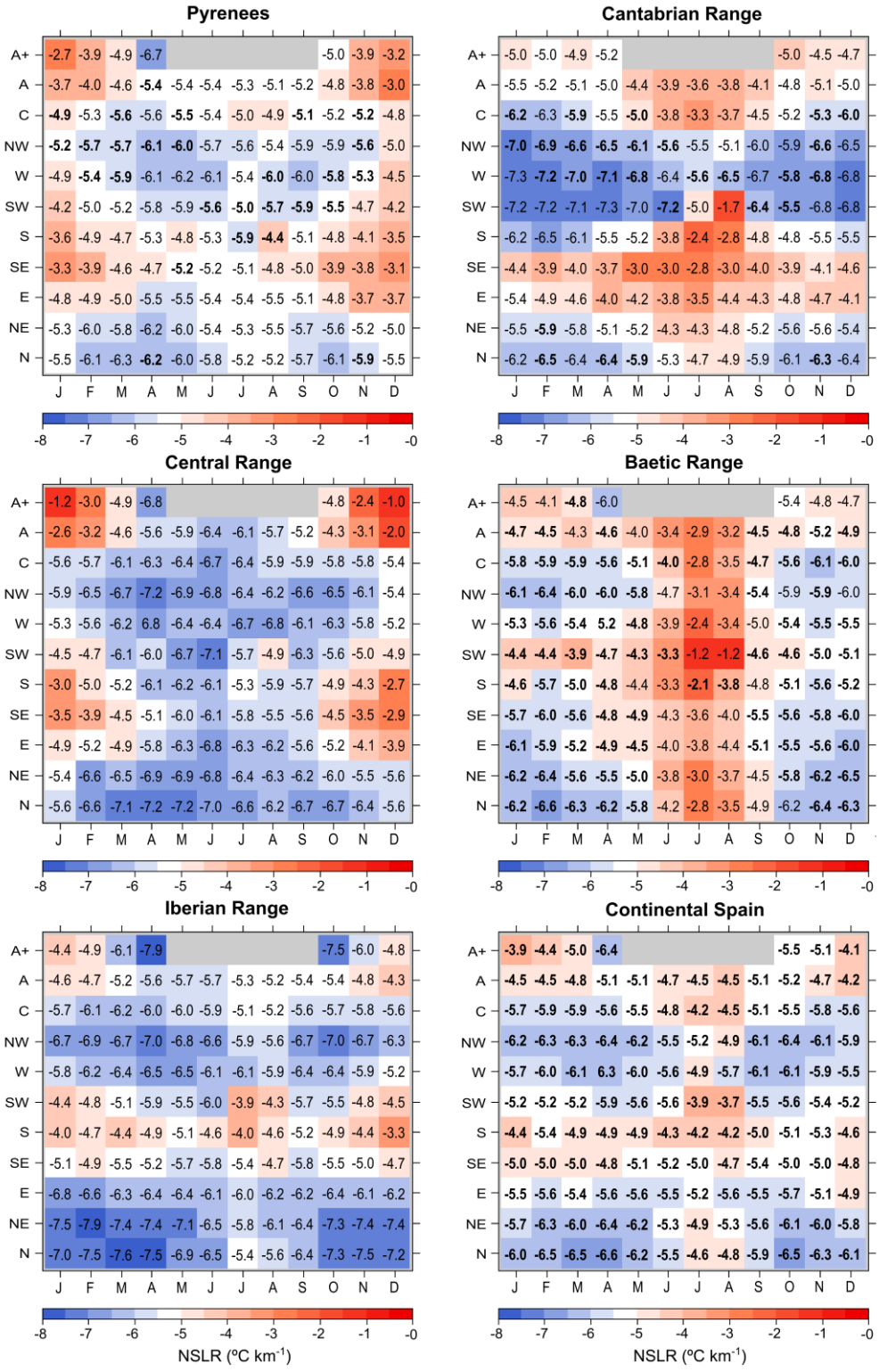

780

781 **Figure 8. Monthly median daily mean near-surface air temperature lapse rate ($NSLR_{dmean}$: °C km^{-1}) for**
782 **different months and synthetized circulation weather types (CWTs). Accuracy ± 1 °C (95% confidence**
783 **interval) is represented by bold values.**

784

785 **Table 1. Elevations and dimensions of the study areas.**

STUDY AREA	DIMENSIONS	ELEVATION RANGES (m a.s.l.)	ELEVATION DISTRIBUTION (m a.s.l., in %)					
			< 500	500 to 1000	1000 to 1500	1500 to 2000	2000 to 2500	> 2500
Pyrenees	412 × 80 km (≈ 75,000 km^2)	Coastline (0) Aneto Peak (3404)	43.62	29.97	13.02	7.54	4.85	1.00
Cantabrian Range	300 × 216 Km (≈ 65,000 km^2)	Coastline (0) Torre Cerredo Peak (2648)	13.96	57.75	22.28	5.77	0.24	In.
Central Range	320 × 200 km (≈ 65,000 km^2)	Tagus river (190) Almanzor Peak (2592)	14.71	65.55	16.28	3.13	0.33	In.
Baetic Range	320 × 290 km (≈ 93,000 km^2)	Coastline (0) Mulhacén Peak (3479)	23.28	56.73	16.00	3.20	0.55	0.24
Iberian Range	160 × 90 and 240 × 200 km (≈ 65,000 km^2)	Coastline (0) Moncayo Peak (2314)	14.16	38.73	42.72	4.37	0.02	0

786

787 **Table 2. Proposed Monthly and CWTs near-surface air temperature lapse rate (NSLR: °C km^{-1}) reference**
788 **values.**

ZONAL REFERENCE Near-surface air temperature lapse-rate ($NSLR_{dmean}$)						
	Pyrenees	Cantabrian Range	Central Range	Baetic Range	Iberian Range	Continental Spain
Zonal	–5.17	–5.22	–5.78	–4.83	–5.79	–5.28
MONTHLY REFERENCE Near-surface air temperature lapse rate ($NSLR_{dmean}$)						
Month	Pyrenees	Cantabrian Range	Central Range	Baetic Range	Iberian Range	Continental Spain
Jan	-4.33	-6.02	-4.10	-5.28	-5.49	-5.16
Feb	-4.97	-6.03	-4.98	-5.58	-5.88	-5.50
Mar	-5.22	-5.80	-5.48	-5.17	-6.00	-5.47
Apr	-5.71	-5.60	-6.28	-5.36	-6.28	-5.80
May	-5.66	-5.12	-6.51	-4.83	-6.19	-5.58
Jun	-5.45	-4.25	-6.71	-3.94	-5.99	-5.09
Jul	-5.21	-4.02	-6.36	-3.03	-5.44	-4.67
Aug	-5.19	-4.28	-6.01	-3.58	-5.45	-4.78
Sep	-5.34	-4.74	-5.82	-4.79	-5.80	-5.39
Oct	-5.21	-5.57	-5.29	-5.31	-5.79	-5.54

Nov	-4.72	-5.82	-4.78	-5.59	-5.78	-5.47
Dec	-4.16	-5.93	-3.92	-5.42	-5.28	-5.15
SYNOPTICAL REFERENCE (by Circulation Weather Types CWT) Near-surface air temperature lapse rate ($NSLR_{dmean}$)						
CWT	Pyrenees	Cantabrian Range	Central Range	Baetic Range	Iberian Range	Continental Spain
N	-5.75	-5.82	-6.70	-5.29	-6.81	-5.91
NE	-5.52	-5.04	-6.43	-4.62	-6.83	-5.63
E	-5.16	-4.20	-5.85	-4.86	-6.25	-5.49
SE	-4.55	-3.65	-4.85	-5.31	-5.34	-5.02
S	-4.63	-5.58	-4.98	-5.08	-4.57	-4.98
SW	-5.00	-7.07	-5.39	-4.65	-5.09	-5.37
W	-5.58	-6.92	-5.97	-5.23	-6.06	-5.88
NW	-5.71	-6.45	-6.52	-5.69	-6.63	-6.10
C	-5.20	-4.81	-6.13	-4.84	-5.63	-5.15
A	-4.79	-4.62	-4.92	-4.32	-5.25	-4.79
A+	-3.55	-4.87	-2.29	-4.58	-4.97	-4.30

Table 3. MAEs (°C) derived for the proposed NSLRs by season, based on 20% of the stations.

Mean Absolute Error (MAE, in ºC) derived of proposed NSLR application by seasons (test: 20% of stations)										
NSLR	PYRENEES					CANTABRIAN R.				
	D–J–F	M–A–M	J–J–A	S–O–N	Mean	D–J–F	M–A–M	J–J–A	S–O–N	Mean
MELR	1.90	1.33	1.42	1.49	1.54	1.68	1.62	2.06	1.64	1.75
ZONAL	1.62	1.25	1.27	1.30	1.36	1.68	1.49	1.64	1.51	1.58
MONTHLY	1.58	1.23	1.26	1.29	1.34	1.64	1.49	1.52	1.49	1.54
CWT	1.57	1.23	1.27	1.28	1.34	1.60	1.41	1.55	1.42	1.50
MON - CWT	1.53	1.21	1.26	1.26	1.32	1.55	1.39	1.46	1.40	1.45
NSLR	CENTRAL R.					BAETIC R.				
	D–J–F	M–A–M	J–J–A	S–O–N	Mean	D–J–F	M–A–M	J–J–A	S–O–N	Mean
MELR	2.55	1.56	1.50	1.87	1.87	1.61	1.66	2.18	1.54	1.75
ZONAL	2.21	1.58	1.59	1.69	1.77	1.52	1.51	1.70	1.42	1.54
MONTHLY	2.02	1.51	1.49	1.65	1.67	1.50	1.51	1.58	1.40	1.50
CWT	2.02	1.51	1.54	1.63	1.68	1.50	1.49	1.71	1.42	1.53
MON - CWT	1.82	1.45	1.48	1.56	1.58	1.47	1.48	1.56	1.39	1.48
NSLR	IBERIAN R.					CONTINENTAL SPAIN				
	D–J–F	M–A–M	J–J–A	S–O–N	Mean	D–J–F	M–A–M	J–J–A	S–O–N	Mean
MELR	2.08	1.59	1.67	1.66	1.75	1.72	1.53	1.81	1.52	1.65
ZONAL	1.95	1.59	1.58	1.59	1.68	1.60	1.47	1.63	1.43	1.53
MONTHLY	1.92	1.57	1.57	1.59	1.66	1.60	1.46	1.61	1.43	1.53
CWT	1.82	1.51	1.59	1.52	1.61	1.57	1.44	1.63	1.42	1.52
MON - CWT	1.78	1.48	1.54	1.50	1.58	1.56	1.43	1.60	1.41	1.50